Jambura Physics Journal

THE EFFECT OF HYDROTHERMAL TEMPERATURE AND UREA DOPING TIME ON THE OPTICAL PROPERTIES OF LEMONGRASS-BASED CARBON NANOPARTICLES (CNPs)

Rahmaniah Nalwi[1], Akhiruddin Maddu[2], Mersi Kurniati[2], Jumardin[3*]

[1] Center for Quality Assurance Group (GPM), Faculty of Agriculture and Forestry, West Sulawesi University. Jalan Prof. Dr. Baharuddin Lopa, S.H, West Sulawesi, Majene 91412, Indonesia.

[2] Pyhiscs Department, Faculty of Mathematics and Natural Sciences, IPB University. Jalan Raya Dramaga, West Java, Bogor 16680, Indonesia.

[3] Physics Department, Faculty of Science and Technology, Alauddin State Islamic University of Makassar, Jalan Sultan Alauddin No.63, South Sulawesi, Gowa 92113, Indonesia.

*Email: jumardin.jumardin@uin-alauddin.ac.id

ARTICLE INFO

ABSTRACT

Carbon Nano Particles (CNPs) sourced from spiced lemongrass have been produced by the hydrothermal method at hydrothermal temperatures of 120, 140, 160 and 180 ^{0}C. The Stokes energy shift occurs due to this absorption transition and the spectrum width is determined by the electronic transition from one energy state to another. This event occurs due to the difference in energy between the two adjacent states due to the smaller vibrational state when compared to the electronic state of the CNPs. The carbon nanoparticles (CNPs) size measurement results showed a peak value of 38.63 nm. Functional group analysis by FTIR spectroscopy showed that the CNP consists of C=C, C-O, OH and C-N-C bonds. The Urbach energy (Eu) increased with increasing hydrothermal synthesis temperature at two hours (0.13, 0.16, 0.19 and 0.29) eV and three hours (0.12, 0.17, 0.19 and 0.28) eV. The bandgap energy (Eg) decreased with increasing hydrothermal synthesis temperature to two hours (2.30, 2.24, 2.00 and 1.92) eV and three hours (2.22, 2.20, 2.17 and 1.75) eV. The expansion of urea as a nitrogen source was carried out at a aqueous temperature of 180 ^{0}C for

2 hours and 3 hours within the blend of CNPs. The addition of urea gave a different effect on the bandgap energy (Eg) and Urbach energy (Eu) on the two CNPs. The bandgap energy (Eg) both increased from two hours (1.92 eV) to three hours (2 .22 eV), while urbach energy (Eu) decreased for a duration of two hours (3.336 eV) to three hours (3.330 eV) after adding urea. hydrothermal temperature due to synthesis time so that the structure of the CNPs becomes more stable and homogeneous.

1. Introduction

Research related to Carbon Nano Particles (CNPs) which include methods of synthesis, carbon sources, optical properties and their applications has been continuously carried out over the last fifteen years (Jelinek, 2017). Its properties which resemble those of inorganic semiconductor nanoparticles make this carbon-based material an opportunity to replace or be used together with inorganic semiconductors in its application (Choi et al., 2018). The joint use of CPNs and TiO2 or CNPs and ZnO semiconductors in photocatalyst applications has been shown to increase the efficiency of absorption of ultraviolet and visible light (Truskewycz et al., 2022). In addition, the strong and stable luminescence of CNPs has also become the main attraction for the development of this research and has been used in biochemical sensor applications (Dhenadhayalan & Lin, 2015), bioimaging (Jhonsi, 2018) and also biocompatible fluorescent inks (Dias et al., 2019).

In common, there are two approaches for CNPs union, top-down and bottom-up. Aqueous union may be a simple bottom-up strategy for synthesizing carbon nanoparticles, the essential rule of which is that chemical responses take put in a fluid medium at temperatures over 100 ^{0}C (Sedira & Mendaci, 2020) and pressures of 1 bar (Nhàn et al., 2021). Synthesis time (duration), hydrothermal temperature, carbon source and the treatment before and after synthesis will affect the size, structure, and optical properties of CNPs which will also affect their utilization (Nammahachak et al., 2022a). CNPs which are sourced from natural materials are an opportunity to be applied in biological systems (Liang et al., 2019) because they are low in toxicity (Yuan et al., 2019). CNPs synthesized from ginger has been appeared to hinder the expansion of liver cancer cells (Li et al., 2014), CNP in coriander leaves can be used as an antioxidant, sensor and bioimaging tool (Sachdev & Gopinath, 2015), and potato-based CNPs can act as probes for imaging epithelial tissue cells (Mehta et al., 2014).

Hydrothermal reaction parameters, including temperature and time, carbon sources, reagents, and dopants, affect the optical properties of CNPs. In this study, the hydrothermal method was used to hydrothermally synthesize CNPs for 2 h and 3 h, and the impacts of temperature and aqueous time on the gotten optical properties were analyzed. Synthesis was carried out with the addition of urea as a nitrogen source which effectively reduced the bandgap energy and increased the fluorescence intensity (Li et al., 2019). In this study, the addition of urea was carried

out on the sample for a reaction temperature of 180 °C with the assumption that the highest fluorescence quantum yield was produced from the high temperature of the hydrothermal reaction (Meiling et al., 2016).

In this research, Lemongrass (*Cymbopogon citratus*) stems were used as a carbon source. Lemongrass is a herbaceous plant that is commonly used in countries with tropical climates, especially in the Southeast Asian region. Lemongrass contains phytochemical compounds in the form of flavonoids (Nurinnafi'a et al., 2022), phenolics (Falah et al., 2015), terpenoids (Balfas & Rahmawati, 2022), and essential oils, and chemical composition consisting of carbohydrates, proteins, fats, and fiber (Pratiwy et al., 2019). The many of syntheses of CNPs, there have been no related studies using citronella as a carbon source. Phytochemical compounds and chemical compositions which are the source of carbon in lemon grass produce CNPs that are different from their original properties and will also be different from CNPs produced from other sources.

Hydrothermal methods are methods of synthesis of CNP materials using single or heterogeneous reactions in aqueous solutions at high temperatures (T > 25 °C) and pressures > 100 kPa. The hydrothermal method was chosen because it is relatively simple and does not require equipment complex and expensive (Anh Tuan et al., 2021), but it also has several advantages such as fast heating (Ruiz-Jorge et al., 2021), fast reaction (Auyoong et al., 2013), better results, high purity and efficiency, transformation energy (Babu et al., 2023). The selection of temperatures aims to control the optical properties and intensity of luminescence of CNPs (Kapitonov et al., 2018). The use of hydrothermal temperatures refers to several studies, temperatures of 140 °C (Aydin et al., 2022), temperatures of 160 °C (Carvalho et al., 2019), temperatures 180 °C (Nammahachak et al., 2022b). Hydrothermal time is one of the factors that affect the synthesis of CNPs. The longer the hydrothermal time, the more fluorescence intensity and wavelength produced will increase (Suzuki et al., 2021). The variation of hydrothermal time used in this study was 2 and 3 hours to determine the effect of hydrothermal time on the synthesis results.

2. Method

The materials used were lemongrass stems as a carbon source, distilled water as a solvent, urea ($CO(NH_2)_2$) as a nitrogen source, filters 0.45 μm and 0.2 μm. The first step is to synthesize CNPs with variations in temperature (120, 140, 160 and 180) °C and duration (2 and 3) hours respectively. Synthesis of CNPs by hydrothermal method using Reactor Controller Type 4848 (Parr Instrument Company). The layers of fresh lemongrass stems were separated into strands, washed and wiped in each layer, then washed again using distilled water, then drained, and weighed using a digital scale to obtain 12 grams of lemongrass. The lemongrass is cut to deliver a littler measure of almost (0.2 x 0.4 x 0.6) cm. Lemongrass was put in a Vessel Reactor with a volume of 600 ml and 50 ml of refined water was included to it, the tube was closed and warmed at 120 °C for 2 hours. After warming, continue with normal cooling. This procedure was repeated at different temperatures (140, 160 and 180)

^{0}C for 2 hours. The same procedure was carried out for hydrothermal for 3 hours (Liu et al., 2012).

The second stage is synthesizing CDs with the addition of urea ($CO(NH_2)_2$). Synthesis was carried out with the same procedure as CDs without adding urea. This procedure is carried out by adding 0.02 grams of urea. The hydrothermal synthesis was performed using the Small Bench Top Reactor and reactor controller. The hydrothermal product was filtered through a 0.45 µm pore filter and the large particles were filtered. centrifuge at 18,000 rpm for (0-30) min at room temperature. The centrifuge that was used was Himac CR 21G. Fill the bottle with CDs sample, for a 50 mL volume bottle with a maximum capacity of eight bottles for one centrifugation. Insert the bottles containing the CDs samples into the centrifuge container in a balanced position (2, 4, 6 and 8 bottles per centrifugation), adjusting the temperature, speed and spin time required. CDs from the centrifugal products were stored at room temperature for further characterization.

Figure 1 shows the method for synthesizing CPNs using a hydrothermal reactor. Figure 1 briefly shows the synthesis flow. The first step is to prepare the ingredients needed, namely the lemongrass that has been cut into small pieces. The results of these small pieces are put into the Autoclave Vessel. The temperature used according to the research method. The initial temperature used was 120 ^{o}C for 2 hours, followed by 140 ^{o}C, 160 ^{o}C and 180 ^{o}C. This method is also performed for the 3 hour time parameter with the same temperature sequence. The hydrothermal results were filtered through the sediments and the optical, FTIR, and particle size properties of the CNPs are described.

UV-Vis absorption spectroscopy measurements were performed using a UV-Vis spectrophotometer (Ocean Optics USB-4000). Fluorescence spectroscopy was
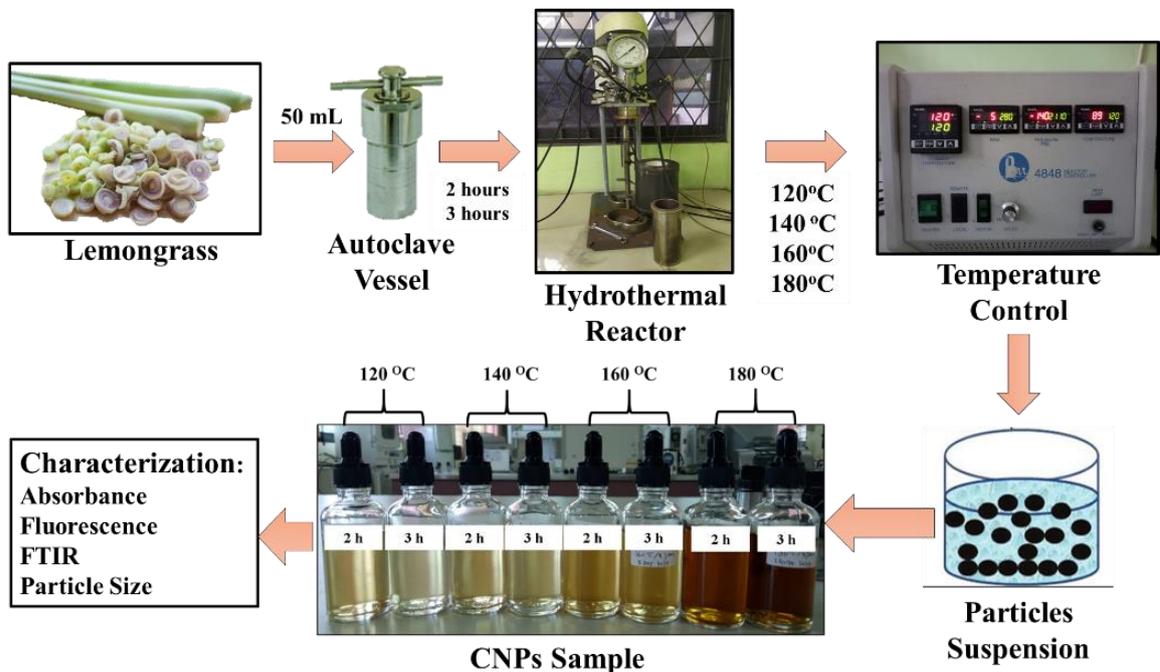
Figure 1. Synthesis of CNPs by hydrothermal method at temperature and time control

performed using a fluorescence spectrometer (Ocean Optics USB-4000). Infrared spectra were recorded on an ABB-MB$_{3000}$ FTIR spectrometer. The Zetasizer Ver.7.11 Malvern Instruments Ltd was used to measure the size distribution of the CNPs. CNPs were sifted through a 0.2 μm channel layer some time recently estimation. All estimations were performed at room temperature. The bandgap energy (Eg) can be calculated from measurements of the absorption spectrum using the Tauc Plot method in equation (1). The assimilation coefficient (α) is utilized to decide the Urbach vitality parameter (Eu) comparing to the move between the extended valence band state and the neighborhood conduction band state. The Urbach energy (Eu) is determined on the graph of Ln(α) compared to the photon energy (hv) by equation (2). hv is the photon energy as a function of the frequency and wavelength shift (λ).

$$(\alpha h v)^n = A(h v - Eg) \qquad (1)$$

$$\ln \alpha = \ln \alpha_0 + \left(\frac{hv}{E_u} \right) \qquad (2)$$

The esteem of h is Planck's steady, v is the recurrence of light, α is the retention coefficient, A is the optical steady, and Eg is the bandgap energy (Pathak et al., 2012). The control esteem of n relates to the electronic properties of the bandgap, where n=2 for coordinate moves and n=1/2 for roundabout electronic moves. Based on this proportionality, the bandgap energy can be determined by constructing a curve between hv and $(\alpha hv)^{1/2}$. (Suram et al., 2016). In this study, the calculation of the bandgap energy uses the value n = 2 by assuming that the electronic transitions that occur in the absorption band are indirect (Zeng et al., 2017). The Urbach energy (Eu) is determined from the linear slope of the absorption coefficient curve (Ln (α)-(hv)) or as the reciprocal of the slope of the linear part of the diagram between Ln (α)-(hv).

The Stokes shift is a quantized energy transition caused by the radiant electric field with electrons. This incident absorbs light energy from the laser at a certain wavelength and re-emits the light energy at a larger wavelength (Zhang et al., 2021). The contrast in energy between the excitation and emission groups is called the Stirs move. The bigger the ΔE, the bigger the Stokes move, which causes the optical bandgap to broaden. Stokes shift energy is calculated by using the equation:

$$\Delta E = E_{\text{Excitation}} - E_{\text{Emission}} \qquad (3)$$

ΔE is the shift in Stokes energy, E_{Emission} is the energy (hv) of the peak wavelength of the fluorescence and $E_{\text{Excitation}}$ is the energy (hv) of the peak wavelength of the absorbance.

3. Result and Discussion

Synthesis of CNPs made from lemongrass using the hydrothermal method showed that the temperature and hydrothermal duration affected the optical properties and energy produced. At a duration of 2 and 3 hours, there is a difference in the value of the intensity of the absorption of CDs absorption to the wavelength of UV light

based on hydrothermal temperature. For 2 hours there was a change in the absorbance value between 120 °C, 140 °C and 160 °C which tended to show a change in the peak wavelength value linearly (Figure. 2A). Meanwhile, the fluorescence intensity occurs at a wider wavelength than the hydrothermal temperature of 180 °C, while the hydrothermal temperature of 120 °C, 140 °C, and 160 °C tends to have the same emission spectrum bandwidth with the highest intensity produced by CDs with a temperature of 120 °C (Figure. 2B).

For a duration of 2 hours, the bandgap energy of CDs of lemongrass stems was in the range of (2.30, 2.24, 2.20 and 1.92) eV (Figure. 2C), while the energy of urbcah (Eu) was (0.13, 0.16, 0.19 and 0.29) eV for temperatures of (120, 140, 160, 180) ^{0}C for two hours of hydrothermal duration (Figure. 2D). The bandgap energy (Eg) of CDs synthesized within 2 h decreased with increasing hydrothermal temperature, while the Urbach energy (Eu) increased with increasing hydrothermal temperature.

There was a band move within the emission range when the hydrothermal duration was increased to 3 hour, UV light absorption (Figure 3A) and fluorescence intensity (Figure 3B) increased at the synthesis temperature of 160 ^{0}C and 180 ^{0}C. Emission spectral peaks around 500 nm with excitations of 400 – 410 nm were also produced
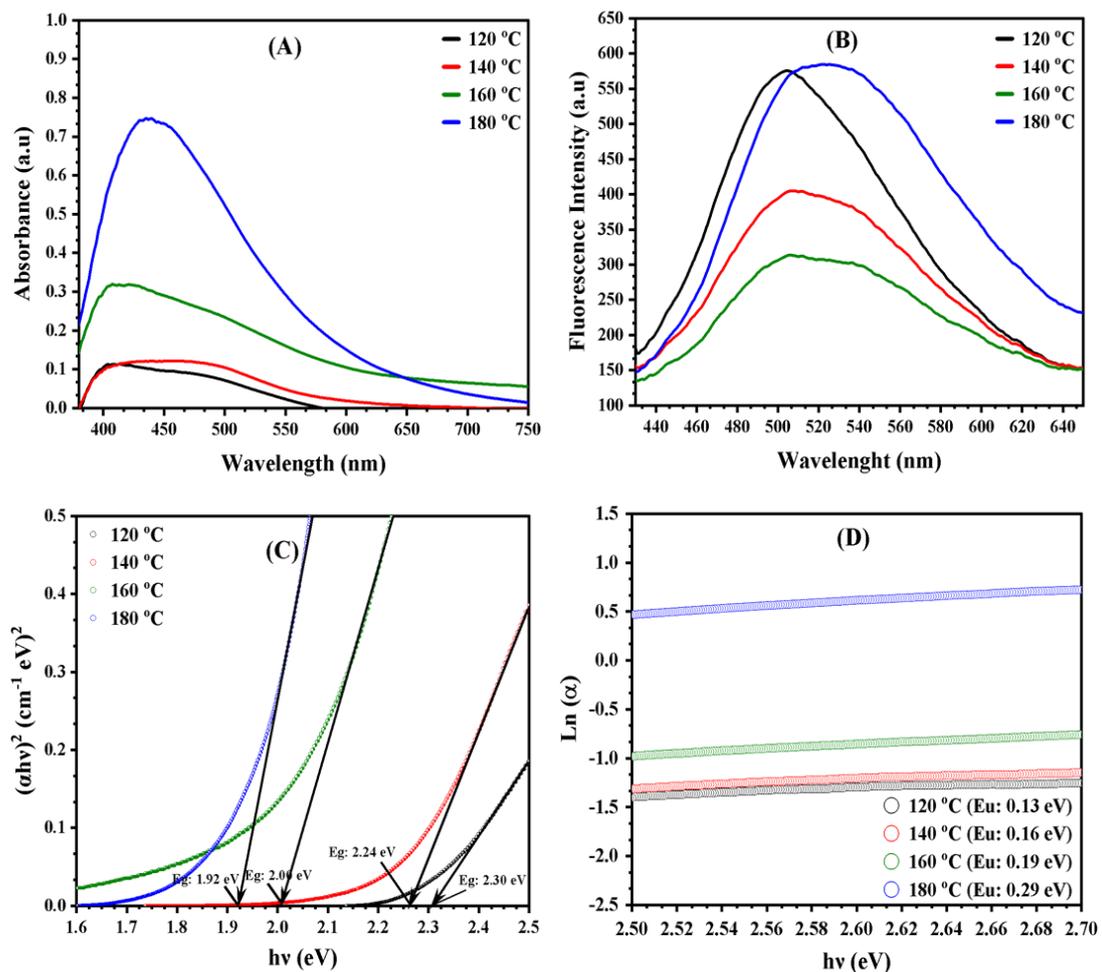
Figure 2. Spectra of (A) absorption, (B) fluorescence intensity, (C) Eg and (D) Eu of 2-hour samples.
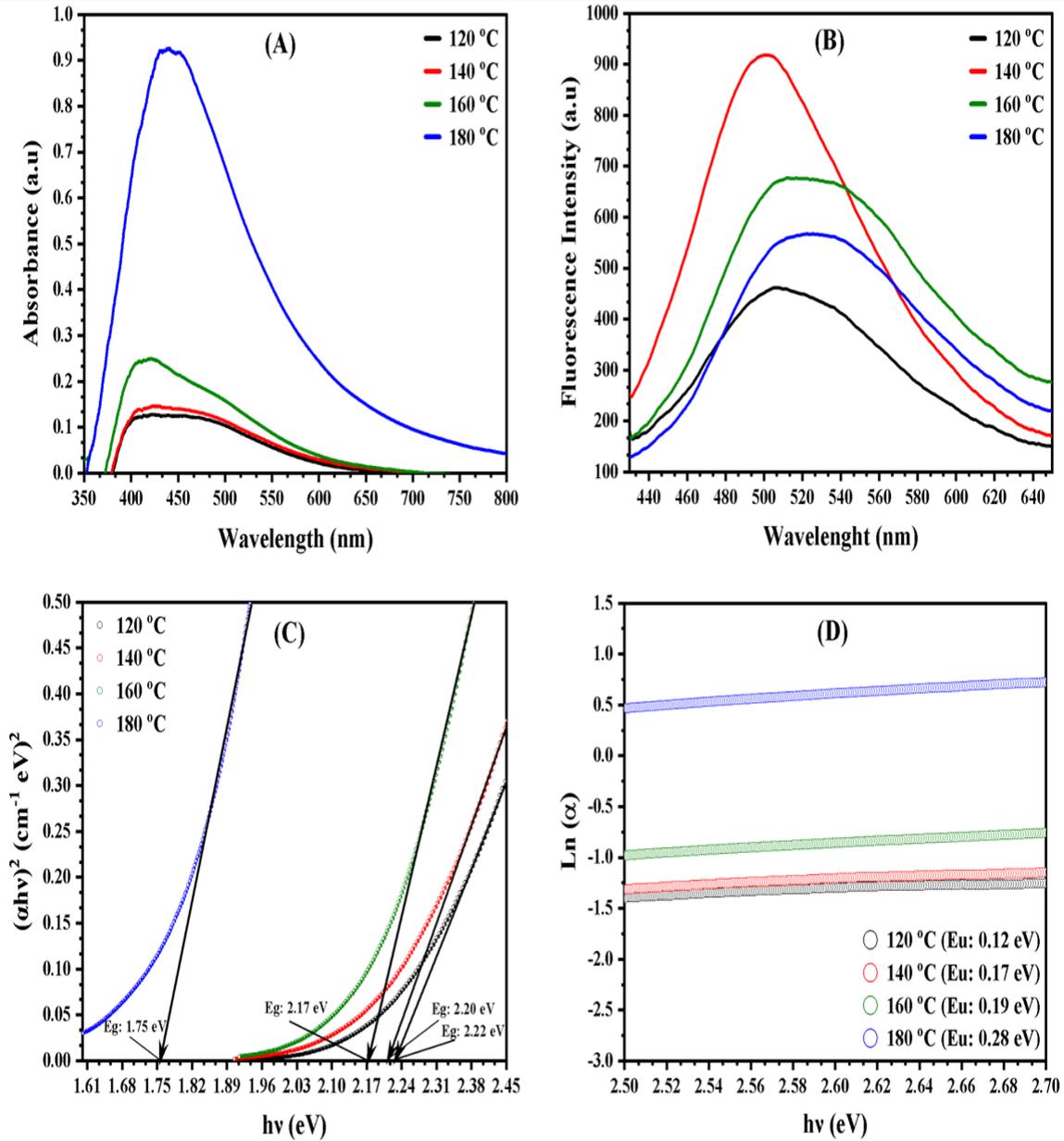
Figure 3. Spectra of (A) absorption, (B) fluorescence intensity, (C) Eg and (D) Eu of 3-hour samples

in several studies (Zhang et al., 2013). CNPs that were synthesized for 3 hours experienced an increase in energy gap as the hydrothermal temperature increased with the highest energy band gap of 2.22 eV (120 ^{0}C) , 2.20 eV (140 ^{0}C), 2.17 eV (160 ^{0}C) and 1.75 eV (180 ^{0}C) (Figure 3C). Differences in the energy gaps of CNPs can be caused by variations in nanoparticle size, shape, and surface structure.

Bandgap (Eg) will decrease with increasing nanoparticle size (Choi et al., 2018). The urbach energy (Eu) increases at 120 ^{0}C (0.12 eV), 140 ^{0}C (0.17 eV) and 160 ^{0}C (0.19 eV). Meanwhile, at 180 ^{0}C it dropped to 0.28 eV, this happened because the CDs absorption coefficient increased and the energy gap (Eg) decreased. Urbach energy (Eu) values are plotted on a plot of Ln (α) versus photon energy (hv). (Figure 3D)

using equation (2), while the energy gap (Eg) value using the Tauc Plot method in equation (1).

Table 1. Bandgap energy (Eg) and Urbach energy (Eu) values based on synthesis hydrothermal temperature.

Synthesis Temperature (°C)	Eg (eV)		Eu (eV)	
	2 h	3 h	2 h	3 h
120	2.30	2.22	0.13	0.12
140	2.24	2.20	0.16	0.17
160	2.00	2.17	0.19	0.19
180	1.92	1.75	0.29	0.28

Table 1 is the result of optical parameter calculations based on hydrothermal temperature. Table 1 is the value of the energy gap (Eg) and energy urbach (Eu). This value is affected by temperature and hydrothermal time, indicating that the higher the temperature, the higher the Urbach energy (Eu) value, while the lower the energy gap (Eg) value is, the higher the temperature at two and three hours. The Urbach energy (Eu) is the distinction in photon energy (hv) between the retention groups found within the locale between the valence band and the conduction groups. Urbach energy (Eu) can also occur as a result of the process of cation distribution in the synthesis method due to the influence of hydrothermal temperature, causing cation migration. The decrease in Urbach energy (Eu) and band energy (Eg) in citronella synthesis under hydrothermal temperature treatment
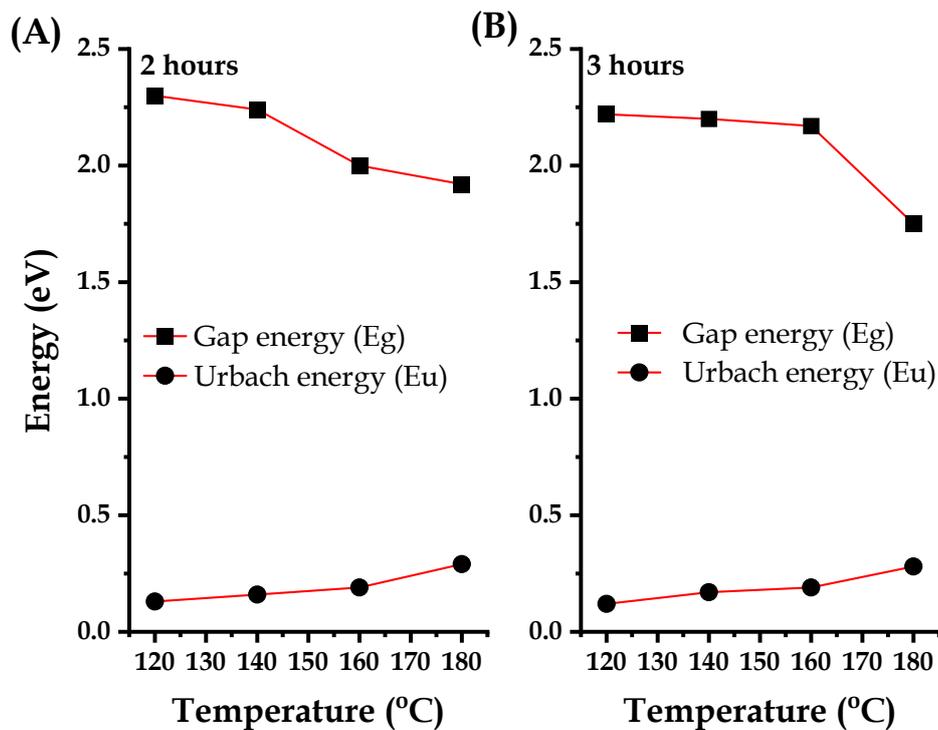
Figure 4. Graph of temperature relationship with (A) 2-hour and (B) 3-hour of Eg and Eu.

may be due to the increase in molarity to make it more stable and homogeneous. The increase in Urbach energy (Eu) and energy gap (Eg) is due to the increase in structural disorder in the molecular properties of this synthesis method. The irregularity is due to the increasing hydrothermal temperature. The high Urbach energy (Eu) and low gap energy (Eg) also indicate that the sample has a low density, as indicated by the UV absorption intensity value, which increases with increasing hydrothermal temperature.

Figure 4 is the relationship between Urbach energy (Eu) and bandgap energy (Eg) with changes in synthesis time and temperature. When the temperature and time increase in hydrothermal, the value of the energy gap (Eg) decreases. This occurs because the concentration of moving atomic bonds absorbs the photon's energy, sharpening the exponential band tails of the conduction and valence bands. As a result, the bandgap (Eg) value becomes smaller. The relationship between bandgap energy (Eg) and Urbach energy (Eu) is shown in Figures 4 (A) and (B). The
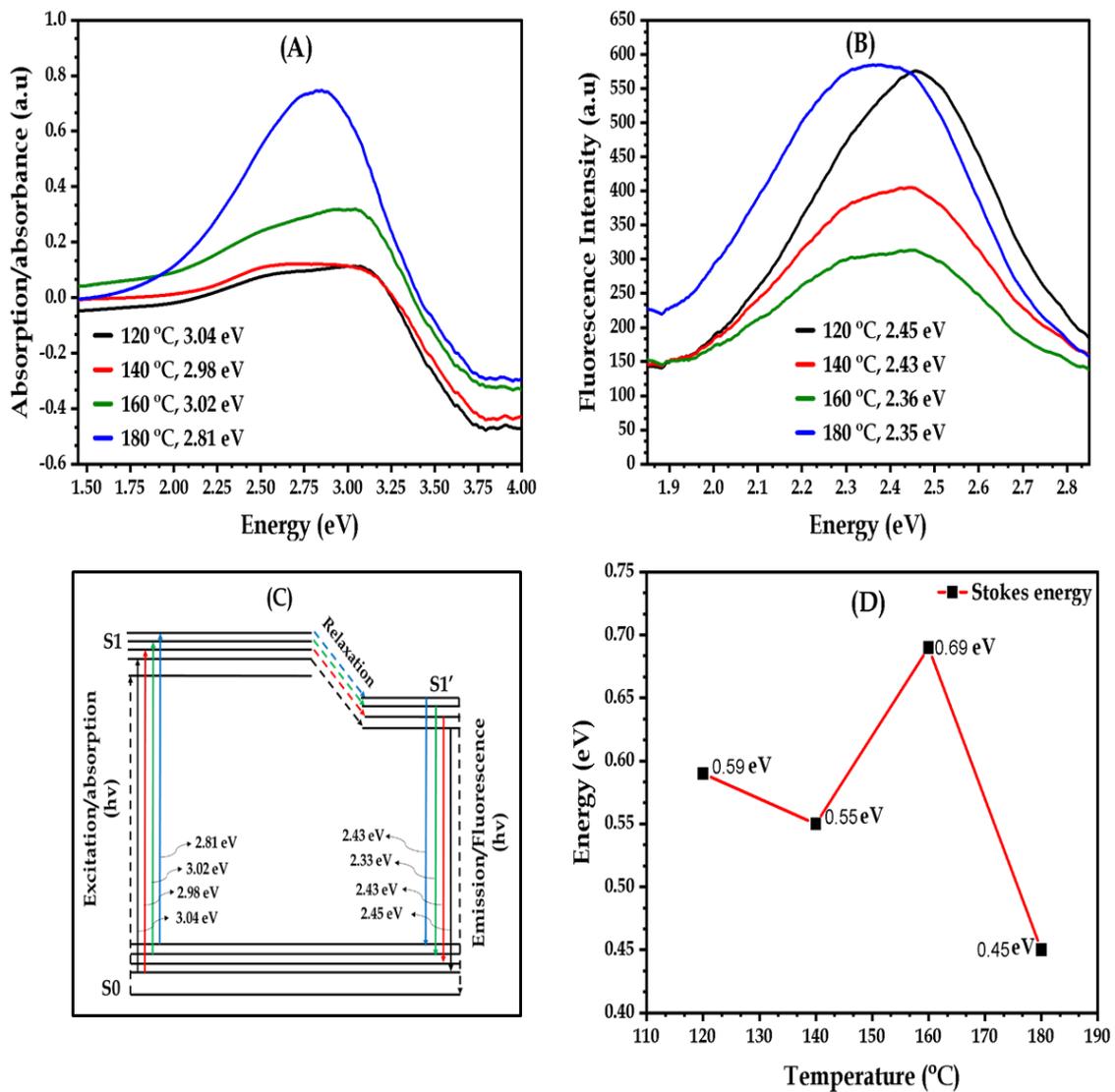
Figure 5. Two-hours sample relationship chart (A) hv to absorbance, (B) hv to fluorescence intensity, (C) fluorescence of mechanism and (D) Stokes energy at hydrothermal temperature
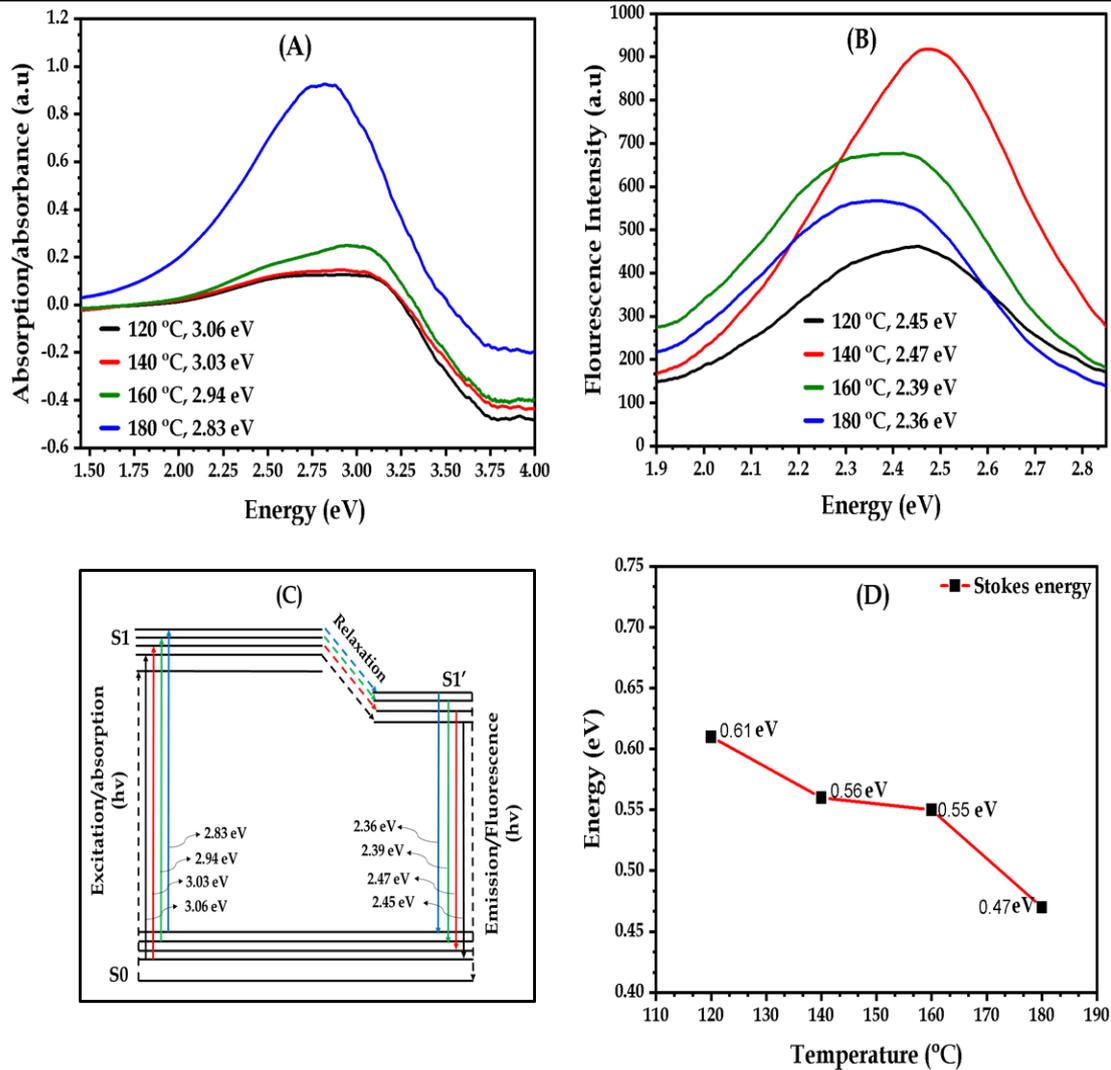
Figure 6. Three-hours sample relationship chart (A) hv to absorbance, (B) hv to fluorescence intensity, (C) fluorescence of mechanism and (D) Stokes energy at hydrothermal temperature.

decreasing value of the trend line is based on the results of the survey (Kré et al., 2010).

Synthesis of carbon nanoparticles (CNPs) made from lemongrass using the hydrothermal method shows that the temperature and hydrothermal duration affect the luminescence of CNPs. For two hours, there was a shift in the emission band towards a longer wavelength at a hydrothermal temperature of 180 °C, while temperatures of (120, 140, and 160) °C tend to have the same emission spectrum bandwidth with the highest intensity being produced by CNPs with a temperature of 120 °C. When the hydrothermal duration was increased to three hours, there was a shift in the emission spectral bands for the synthesis temperature of 160 °C and 180 °C.

In Figures 5 (B) and 6 (B) the energy level of fluorescence emission is smaller in number when compared to the excitation energy (absorbance) in Figures 5 (A) and 6 (A), causing different colors in the excitation and emission stages. In addition, the

wavelength of the emission will always be longer than the wavelength of the excitation. This is caused by the relaxation process. The process can be seen in Figures 5 (C) and 6 (C). The results of the Stokes displacement energy and the analysis curve of the Carbon Nanoparticles (CNPs) after the hydrothermal temperature change can be seen in Figures 5 (A) and 6 (A).

The fluorescence emission is a result of the thermal equilibrium of the excitation state, that is, at the lowest vibrational energy level. Measurement of absorbance and fluorescence intensity after the addition of hydrothermal temperature produces intensity values at different peak wavelengths. The absorbance absorption results have presented the changing peak wavelength values based on the synthesis of hydrothermal temperatures for two and three hours duration. This change indicates that the CNPs molecules in water solvent are stronger in intensity to absorb UV-Vis light at 180 ^{0}C with a time of three hours than the CNPs molecules synthesized in two hours. When the CNPs that have been synthesized for three hours are long, they absorb photon energy so that excitation occurs to the LUMO level. The electrons return to their ground state while emitting light (fluorescent). The CNPs emission photon energy value at 2 hours duration was shown in bland 5 (C) and after three hours of synthesis it was seen in bland 6 (C). This has indicated that the CNPs molecules absorb laser (405±10) nm more strongly as a light source at 3 hours duration than at two hours duration at hydrothermal synthesis temperature.

Figures 5 (C) and 6 (C) show that luminescence events occur in CNPs whose surface is passive due to the presence of energy traps, thus emission stabilization occurs. When the CNPs return to the ground state (S0), they emit energy photons ($E_{Exc.}$), then the emitted photons ($E_{Em.}$) have a smaller energy and longer wavelength than the photons absorbed by the energy absorption ($E_{exc.}$). The difference between the excitation and emission energies ($E_{Exc.} – E_{Em.}$) of CNPs can be seen in figures 5 (D) and 6 (D). Therefore, the CNPs molecules are excited quickly (relaxed) to the lowest vibrational energy level, namely from S1 to S1' due to the energy dissipation of the CNPs (Figure 5 (C) and 6 (C)). So that the fluorescence emission spectrum is independent of the wavelength of the excitation wavelength peak, the emission represents the transition of the molecules from low energy to higher energy, namely HOMO to LUMO, which then falls to a lower energy level and usually occurs as a triplet in the area. HOMO is the highest valence band orbital occupied by an electron, and LUMO is the lowest conduction band orbital not occupied by an electron (Yoosefian et al., 2018). In the analysis of emission levels high-intensity values indicate large amounts the particle falls to a lower energy level. This Stokes shift occurs because the structure of CNPs in the ground state is different when compared to that in the excited state.

Figure 7 (A) is the spectrum of the wavelength of the CNPs transmittance value. The interaction between infrared radiation and CNPs was recorded using an FTIR spectrometer in the medium infrared range (4000 − 400 cm^{-1}). The FTIR spectrum sample measurements used were 3 hours and 180 ^{0}C. This was done because the absorption value of UV light at 3 hours with a temperature of 180 ^{0}C was higher than other measurements. The results show that strain vibration occurs in the absorption band 1636 cm^{-1} which is an aromatic vibration C=C and C=O (Yang et
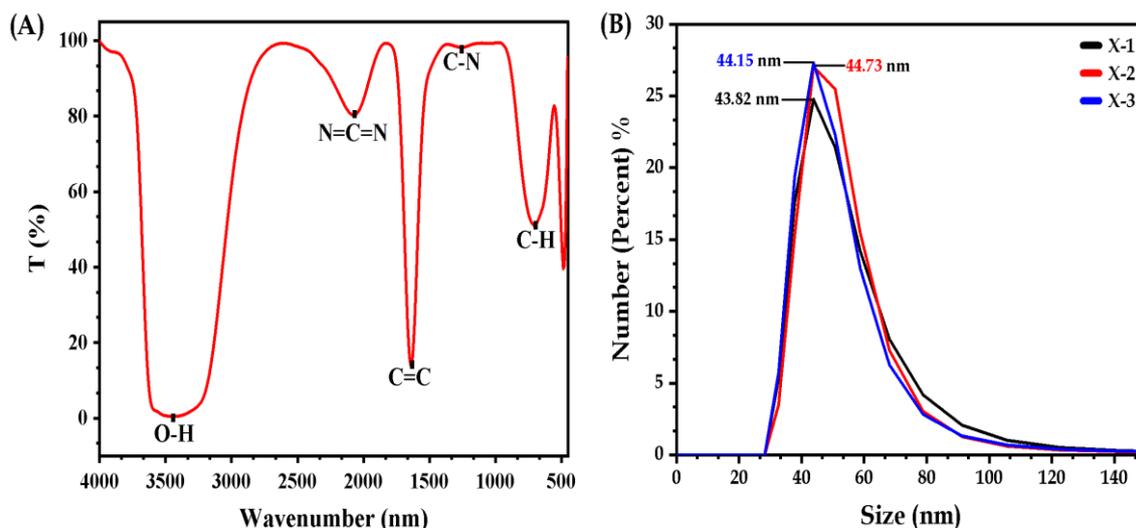
Figure 7. (A) FTIR spectrum of CNPs and (B) Size distribution of CNPs.

al., 2014), 3250 – 3600 with peak 3441 cm^{-1} which is a strain vibration O-H (Ruan et al., 2016), 2075 cm^{-1} vibration strain N=C=N (Stuart, 2004). These vibration peaks are similar to results reported by Yang and colleagues (Yang et al., 2014) . The infrared spectra of various research results differ from one another, especially for CNPs which depend on the carbon source, reaction method and parameters (Ţucureanu et al., 2016). In any case, the electronic move of the carbon center (C=C), which may be a surface useful bunch counting C-O, C=O, and COOH, is the electronic move that starts the fluorescence of CNPs (Khan et al., 2017).

Measure conveyance estimation by energetic light diffusing in figure 7 (B) appeared that CNPs was synthesized at 180 ^{0}C for 3 hours. X-1 is the primary estimation, X-2 is the moment estimation, X-3 is the moment estimation. The average value of nanoparticle size is added up and then divided by the number of repeat measurements that have been carried out. So that the distributed CNPs size values are shown in Figure 6 by presenting X-1 (black graph) with a number intensity of 24.77% (43.82 nm), X-2 (red color graph) with a number intensity of 27.32% (44.73 nm) and X-3 (blue color chart) with an intensity of 27.34%. This indicates that the CNPs produced in this synthesis are not classified as CDs below 10 nm due to other particles in the sample (Wang & Hu, 2014). The average size distribution of the CPNs was 38.63 nm For further purification, dialysis membranes can be used.

Doping, or adding certain elements to CNPs, is a method used to control the photoluminescence properties. The variety of precursors that can be used as a nitrogen source. Use of urea as doping in the synthesis of CNPs which is applied as a temperature sensor (Atabaev et al., 2019). In this study, the addition of urea to the synthesis of CNPs gave a different effect on the optical properties between the hydrothermal durations for two hours and three hours. During the two-hour hydrothermal time, the addition of urea results in a spectral shift of the absorption band towards shorter wavelengths (blue-shift), accompanied by an increase in absorption intensity, On the other hand, the fluorescence emission band spectrum shifts to longer wavelengths (red shift) with decreasing intensity (figure 8 (A)).
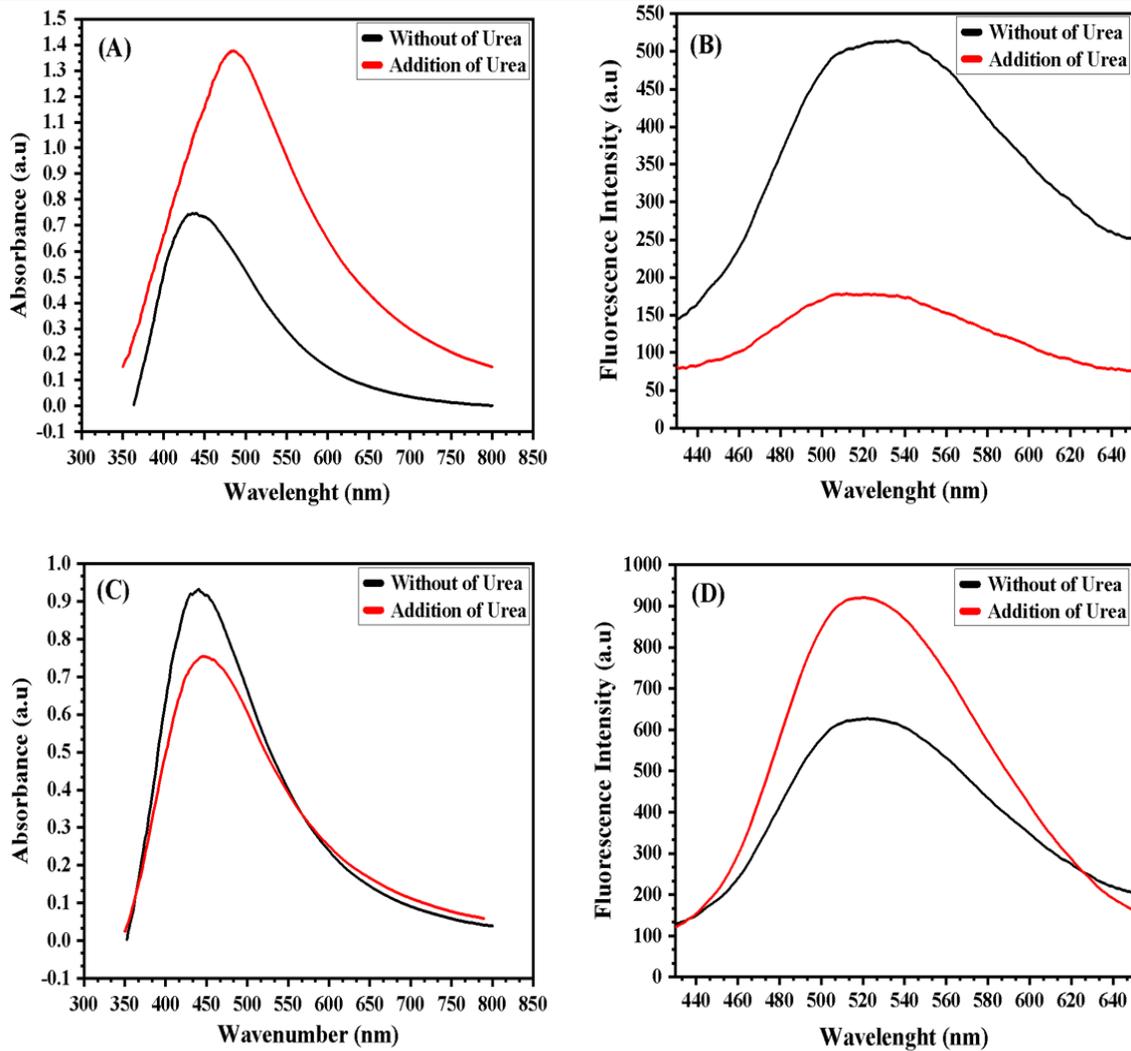
Figure 8. (A) Absorption spectrum, (B) Fluorescence intensity after addition of urea for 2 hours, (C) absorption spectrum and (D) fluorescence intensity after adding urea for 3 hours.

The shift in absorption towards longer wavelengths can be caused by the joining of CNPs and some auxochromes, this was also produced in research conducted by (Atabaev et al., 2019) and also by (Wu et al., 2017). The decrease in quenching intensity can be caused by various processes (Figure. 8 (B)), including a decrease in intensity due to collisions that occur when the fluorophore in an excited state is deactivated due to contact with another molecule (quencher). Some of the molecules that can cause a decrease in intensity (quencher) are oxygen, halogens, amines, and molecules that lack electrons.

The plot using the Tauc method shows that there is a difference in the band gap energy (Eg) between the CNPs without the addition of urea and with the addition of urea. The resulting band gap energies of 1.92 eV and 2.22 eV for CNPs after adding urea resulted in an increase in energy gap after adding urea. (Figure. 9 (C)). This indicates that urea can increase the valence and conduction band energies (Choi et al., 2018) addition of nitrile groups and nitro groups to the carbon point also shows that the energy of the HOMO-LUMO gap is narrowed, resulting in a

HOMO-LUMO gap energy of 1.12 eV. undoped carbon dot and HOMO-LUMO gap energy decrease to 1.05 eV and 1.03 eV for carbon doped with nitro and nitrile groups, respectively. The addition of certain groups to adjust the bandgap is called the bandgap technique, which refers to the concept that molecules with strong electron-withdrawing groups tend to produce low LUMO energy levels (Choi et al., 2018).

The shift in absorption towards longer wavelengths can be caused by the joining of CNPs and some auxochromes, this was also produced in research conducted by (Atabaev et al., 2019) and also by (Wu et al., 2017). The decrease in quenching intensity can be caused by various processes (Figure. 8 (B)), including a decrease in intensity due to collisions that occur when the fluorophore in an excited state is deactivated due to contact with another molecule (quencher). Some of the molecules that can cause a decrease in intensity (quencher) are oxygen, halogens, amines, and molecules that lack electrons.
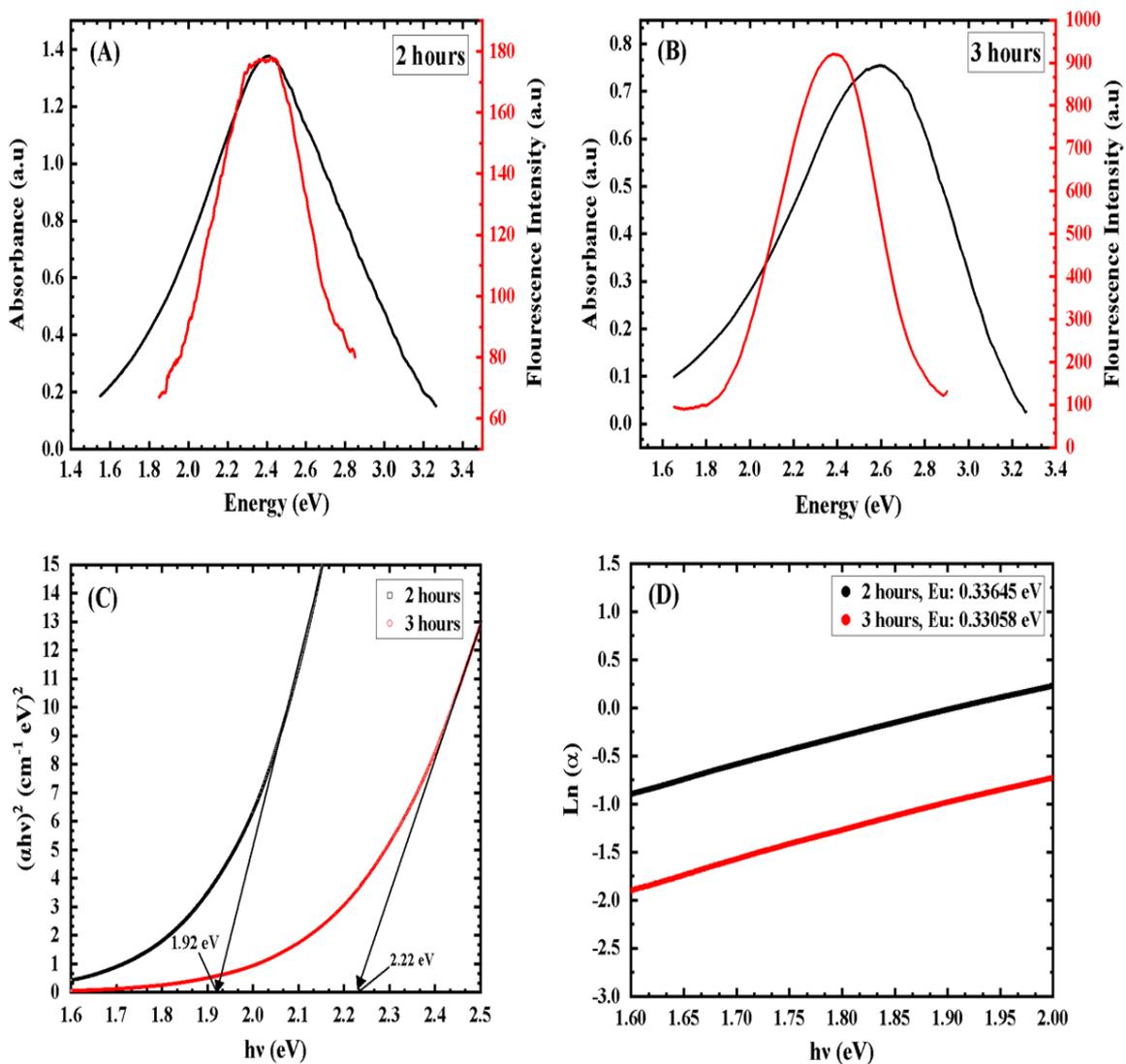
Figure 9. Energy spectrum of (A) absorption, (B) fluorescence intensity, (C) bandgap energy (Eg) and (D) urbach energy (Eu).

The expansion of urea with a hydrothermal time of three hours (figures 8 (C) and 8 (D)) brought about in a blue move of the retention band went with by a diminish in escalated and a blue move of the fluorescence band is wont with by an increment within the retention band with escalated. The move of the fluorescence emission and absorption groups of the CNPs to shorter wavelengths does not appear to be so critical, which may be due to the exceptionally moo nitrogen substance in 0.02 grams of urea. However, nitrogen in urea for three hours of hydrothermal duration showed its role as an effective dopant to increase the fluorescence intensity.

Table 2. Curve slope, Urbach energy (Eu) and bandgap energy (Eg) of CNPs.

Time parameters (hours)	Energy curve (hv) and Ln (α) slope	Eu (eV)	Eg (eV)
2	2.97	0.33645	1.92
3	3.03	0.33058	2.22

The results are summarized in Table 2 at a processing temperature of 180 °C after adding urea during the two and three hour synthesis process. The Urbach energy (Eu) is determined as a function of the photon energy (hv) to Ln (α) as shown in figure 8 (D). Urbach energy (Eu) decreases with the change of synthesis time in the hydrothermal method (two and three hours), while the energy of the valence band increases as the synthesis time increases in the hydrothermal method (Figure. 9 (D)). The Urbach energy (Eu) is calculated as the converse of the incline of the straight portion of the chart between Ln (α) and the energy (hv) (Mishra et al., 2016).

4. Conclusion

Carbo Nano Particles (CNPs) sourced from citronella which has been synthesized by the hydrothermal method produced the highest absorption at the peak wavelength spectrum and the highest fluorescence intensity at 180 ^{0}C and a synthesis time of three hours. Increasing hydrothermal temperature (120 ^{0}C, 140 ^{0}C, 160 ^{0}C and 180 ^{0}C) causes the luminescence peak to shift towards higher wavelengths, while the bandgap energy (Eg) decreases regularly with increasing synthesis temperature for two and three hours. The urbach energy (Eu) increases as the hydrothermal synthesis temperature increases. The Stokes shift shows the transition of absorption energy (absorbance) at the peak of the maximum wavelength and the maximum emission spectrum (fluorescence) value. This Stokes shift occurs because the structure of CNPs in the ground state is different when compared to the excited state. Addition of urea as nitrogen source for the synthesis of CNPs extracted from lemongrass at a synthesis temperature of 180 ^{0}C for three hours could increase the fluorescence intensity. The absorption coefficient (α) increases the bandgap energy (Eg) and decreases the Urbach energy (Eu).

References

Anh Tuan, T., V. Guseva, E., Anh Tien, N., Tan Dat, H., & Vuong, B. X. (2021). Simple and Acid-Free Hydrothermal Synthesis of Bioactive Glass 58 Si O_2-33 Ca O_{-9} P_2 O_5 (wt%). *Crystals*, *11* (3), 283.

Atabaev, T. Sh., Sayatova, S., Molkenova, A., & Taniguchi, I. (2019). Nitrogen-doped carbon nanoparticles for potential temperature sensing applications. *Sensing and Bio-Sensing Research*, *22*, 100253.

Auyoong, Y. L., Yap, P. L., Huang, X., & Abd Hamid, S. B. (2013). Optimization of reaction parameters in hydrothermal synthesis: A strategy towards the formation of CuS hexagonal plates. *Chemistry Central Journal*, *7* (1), 67.

Aydin, S., Ustun, O., Ghosigharehaghaji, A., Tavaci, T., Yilmaz, A., & Yilmaz, M. (2022). Hydrothermal Synthesis of Nitrogen-Doped and Excitation-Dependent Carbon Quantum Dots for Selective Detection of Fe^{3+} in Blood Plasma. *Coatings*, *12* (9), 1311.

Babu, R., Capannelli, G., Bernardini, M., Pagliero, M., & Comite, A. (2023). Effect of varying hydrothermal temperature, time, and sludge pH on sludge solubilisation. *Carbon Resources Conversion*, *6* (2), 142–149.

Balfas, R. F., & Rahmawati, Y. D. (2022). Skrining Fitokimia, Formulasi, dan Uji Sifat Fisik Sediaan Foot Sanitizer Spray Minyak Atsiri Sereh Wangi (Cymbopogon citratrus sp.). *Jurnal Pharmascience*, *9* (1), 11.

Carvalho, J., Santos, L. R., Germino, J. C., Terezo, A. J., Moreto, J. A., Quites, F. J., & Freitas, R. G. (2019). Hydrothermal Synthesis to Water-stable Luminescent Carbon Dots from Acerola Fruit for Photoluminescent Composites Preparation and its Application as Sensors. *Materials Research*, *22* (3), e20180920.

Choi, J., Kim, N., Oh, J.-W., & Kim, F. S. (2018). Bandgap engineering of nanosized carbon dots through electron-accepting functionalization. *Journal of Industrial and Engineering Chemistry*, *65*, 104–111.

Dhenadhayalan, N., & Lin, K.-C. (2015). Chemically Induced Fluorescence Switching of Carbon-Dots and Its Multiple Logic Gate Implementation. *Scientific Reports*, *5* (1), 10012.

Dias, C., Vasimalai, N., P. Sárria, M., Pinheiro, I., Vilas-Boas, V., Peixoto, J., & Espiña, B. (2019). Biocompatibility and Bioimaging Potential of Fruit-Based Carbon Dots. *Nanomaterials*, *9* (2), 199.

Falah, S., Ayunda, R. D., & Faridah, D. N. (2015). *Potential of lemongrass leaves extract (Cymbopogon citratus) as prevention for oil oxidation*.

Jelinek, R. (2017). Carbon-Dot Synthesis. In R. Jelinek, *Carbon Quantum Dots* (pp. 5–27). Springer International Publishing.

Jhonsi, M. A. (2018). Carbon Quantum Dots for Bioimaging. In M. S. Ghamsari (Ed.), *State of the Art in Nano-bioimaging*. InTech.

Kapitonov, A. N., Egorova, M. N., Tomskaya, A. E., Smagulova, S. A., & Alekseev, A. A. (2018). *Hydrothermal synthesis of carbon dots and their luminescence*. 030003.

Khan, W. U., Wang, D., Zhang, W., Tang, Z., Ma, X., Ding, X., Du, S., & Wang, Y. (2017). High Quantum Yield Green-Emitting Carbon Dots for Fe(III) Detection, Biocompatible Fluorescent Ink and Cellular Imaging. *Scientific Reports*, *7* (1), 14866.

Kré, R. N., Moussé, M. L., & Tchétché, Y. (2010). Optical absorption of the hydrogenated evaporated amorphous silicon. *Int. J. Phys. Sci.*

Li, C.-L., Ou, C.-M., Huang, C.-C., Wu, W.-C., Chen, Y.-P., Lin, T.-E., Ho, L.-C., Wang, C.-W., Shih, C.-C., Zhou, H.-C., Lee, Y.-C., Tzeng, W.-F., Chiou, T.-J., Chu, S.-T., Cang, J., & Chang, H.-T. (2014). Carbon dots prepared from ginger exhibiting efficient inhibition of human hepatocellular carcinoma cells. *Journal of Materials Chemistry B*, *2* (28),

Li, J., Ma, S., Xiao, X., & Zhao, D. (2019). The One-Step Preparation of Green-Emissioned Carbon Dots through Hydrothermal Route and Its Application. *Journal of Nanomaterials*, *2019*, 1–10.

Liang, Y., Liu, Y., Li, S., Lu, B., Liu, C., Yang, H., Ren, X., & Hou, Y. (2019). Hydrothermal growth of nitrogen-rich carbon dots as a precise multifunctional probe for both Fe3+ detection and cellular bio-imaging. *Optical Materials*, *89*, 92–99.

Liu, S., Tian, J., Wang, L., Zhang, Y., Qin, X., Luo, Y., Asiri, A. M., Al-Youbi, A. O., & Sun, X. (2012). Hydrothermal Treatment of Grass: A Low-Cost, Green Route to Nitrogen-Doped, Carbon-Rich, Photoluminescent Polymer Nanodots as an Effective Fluorescent Sensing Platform for Label-Free Detection of Cu(II) Ions. *Advanced Materials*, *24* (15), 2037–2041.

Mehta, V. N., Jha, S., Singhal, R. K., & Kailasa, S. K. (2014). Preparation of multicolor emitting carbon dots for HeLa cell imaging. *New J. Chem.*, *38*(12), 6152–6160.

Meiling, T. T., Cywiński, P. J., & Bald, I. (2016). White carbon: Fluorescent carbon nanoparticles with tunable quantum yield in a reproducible green synthesis. *Scientific Reports*, *6* (1), 28557.

Mishra, V., Sagdeo, A., Warshi, K., Rai, H. M., Saxena, S. K., Kumar, R., & Sagdeo, P. R. (2016). *Metastable behavior of Urbach tail states in BaTiO3 across phase transition*.

Nammahachak, N., Aup-Ngoen, K. K., Asanithi, P., Horpratum, M., Chuangchote, S., Ratanaphan, S., & Surareungchai, W. (2022). Hydrothermal synthesis of carbon quantum dots with size tunability *via* heterogeneous nucleation. *RSC Advances*, *12* (49), 31729–31733.

Nammahachak, N., Aup-Ngoen, K. K., Asanithi, P., Horpratum, M., Chuangchote, S., Ratanaphan, S., & Surareungchai, W. (2022). Hydrothermal synthesis of carbon quantum dots with size tunability *via* heterogeneous nucleation. *RSC Advances*, *12* (49), 31729–31733.

Nhàn T. T. T., Uyên P. T. K., Tuấn N. Q., Quang N. K., Toàn Đ. N., Dương Đ. V., Đạt T. N., Liễn P., & Khẩn Đ. T. (2021). *CHẾ TẠO HẠT CACBON NANÔ THEO HƯỚNG TIẾP CẬN XANH BẰNG PHƯƠNG PHÁP THỦY NHIỆT*. *19* (9).

Nurinnafi'a, A. M. U., Artini, K. S., & Permatasari, D. A. I. (2022). Total Flavonoid Content of Lemongrass Leaf (Cymbogoncitratus (DC.) Stapf) Extract and Antioxidant Activity with Frap. *Journal of Fundamental and Applied Pharmaceutical Science*, *3* (1), progress.

Pathak, C. S., Mishra, D. D., Agarwala, V., & Mandal, M. K. (2012). Blue light emission from barium doped zinc sulfide nanoparticles. *Ceramics International*, *38* (7), 5497–5500.

Pratiwy, A. E., Kusumaningrum, I., & Aminullah, A. (2019). UTILIZATION OF LEMONGRASS EXTRACT (CYMBOPOGON CITRATUS) AGAINST THE ANTIOXIDANT CONTENT AND SENSORY PROPERTIES OF DARK CHOCOLATE PRODUCTS. *JURNAL PERTANIAN*, *10* (2), 80.

Ruan, Y., Wu, L., & Jiang, X. (2016). Self-assembly of nitrogen-doped carbon nanoparticles: A new ratiometric UV-vis optical sensor for the highly sensitive and selective detection of Hg $^{2+}$ in aqueous solution. *The Analyst*, *141* (11), 3313–3318.

Ruiz-Jorge, F., Benítez, A., García-Jarana, M. B., Sánchez-Oneto, J., Portela, J. R., & Martínez de la Ossa, E. J. (2021). Effect of the Heating Rate to Prevent the Generation of Iron Oxides during the Hydrothermal Synthesis of LiFePO4. *Nanomaterials*, *11* (9), 2412.

Sachdev, A., & Gopinath, P. (2015). Green synthesis of multifunctional carbon dots from coriander leaves and their potential application as antioxidants, sensors and bioimaging agents. *The Analyst*, *140* (12), 4260–4269.

Sedira, S., & Mendaci, B. (2020). Hydrothermal synthesis of spherical carbon nanoparticles (CNPs) for supercapacitor electrodes uses. *Materials for Renewable and Sustainable Energy*, *9* (1), 1.

Stuart, B. H. (2004). *Infrared Spectroscopy: Fundamentals and Applications*.

Suram, S. K., Newhouse, P. F., & Gregoire, J. M. (2016). High Throughput Light Absorber Discovery, Part 1: An Algorithm for Automated Tauc Analysis. *ACS Combinatorial Science, 18* (11), 673–681.

Suzuki, K., Miyamura, H., & Balachandran, J. (2021). One-pot hydrothermal synthesis of carbon dots-immobilized hydrozincite for ZnO-based nanocomposite lighting applications. *Journal of Asian Ceramic Societies*, *9* (4), 1473–1480.

Truskewycz, A., Yin, H., Halberg, N., Lai, D. T. H., Ball, A. S., Truong, V. K., Rybicka, A. M., & Cole, I. (2022). Carbon Dot Therapeutic Platforms: Administration, Distribution, Metabolism, Excretion, Toxicity, and Therapeutic Potential. *Small*, *18* (16), 2106342.

Ţucureanu, V., Matei, A., & Avram, A. M. (2016). FTIR Spectroscopy for Carbon Family Study. *Critical Reviews in Analytical Chemistry*, *46* (6), 502–520.

Wang, Y., & Hu, A. (2014). Carbon quantum dots: Synthesis, properties and applications. *Journal of Materials Chemistry C*, *2* (34), 6921.

Wu, P., Li, W., Wu, Q., Liu, Y., & Liu, S. (2017). Hydrothermal synthesis of nitrogen-doped carbon quantum dots from microcrystalline cellulose for the detection of Fe^{3+} ions in an acidic environment. *RSC Advances*, *7* (70), 44144–44153.

Yang, X., Zhuo, Y., Zhu, S., Luo, Y., Feng, Y., & Dou, Y. (2014). Novel and green synthesis of high-fluorescent carbon dots originated from honey for sensing and imaging. *Biosensors and Bioelectronics*, *60*, 292–298.

Yoosefian, M., Rahmanifar, E., & Etminan, N. (2018). Nanocarrier for levodopa Parkinson therapeutic drug; comprehensive benserazide analysis. *Artificial Cells, Nanomedicine, and Biotechnology*, *46* (sup 1), 434–446.

Yuan, X., Zhang, X., Sun, L., Wei, Y., & Wei, X. (2019). Cellular Toxicity and Immunological Effects of Carbon-based Nanomaterials. *Particle and Fibre Toxicology*, *16* (1), 18.

Zeng, Z., Zhang, W., Arvapalli, D. M., Bloom, B., Sheardy, A., Mabe, T., Liu, Y., Ji, Z., Chevva, H., Waldeck, D. H., & Wei, J. (2017). A fluorescence-electrochemical study of carbon nanodots (CNDs) in bio- and photoelectronic applications and energy gap investigation. *Physical Chemistry Chemical Physics*, *19* (30), 20101–20109.

Zhang, Y., Zhou, J., Peng, S., Yu, W., Fan, X., Liu, W., Ye, Z., Qi, J., Feng, Z., & Qian, J. (2021). Hot-Band-Absorption-Induced Anti-Stokes Fluorescence of Aggregation-Induced Emission Dots and the Influence on the Nonlinear Optical Effect. *Biosensors*, *11* (11), 468.

Zhang, Y.-Y., Wu, M., Wang, Y.-Q., He, X.-W., Li, W.-Y., & Feng, X.-Z. (2013). A new hydrothermal refluxing route to strong fluorescent carbon dots and its application as fluorescent imaging agent. *Talanta*, *117*, 196–202.